Environmental Pollution 248 (2019) 74–81

Contents lists available at ScienceDirect

Environmental Pollution

journal homepage: www.elsevier.com/locate/envpol

Severe particulate pollution days in China during 2013–2018 and the associated typical weather patterns in Beijing-Tianjin-Hebei and the Yangtze River Delta regions☆

Jiandong Li [a, c], Hong Liao [b, *], Jianlin Hu [b], Nan Li [b]

[a] State Key Laboratory of Atmospheric Boundary Layer Physics and Atmospheric Chemistry (LAPC), Institute of Atmospheric Physics, Chinese Academy of Sciences, Beijing, 100029, China
[b] Jiangsu Key Laboratory of Atmospheric Environment Monitoring and Pollution Control, Jiangsu Collaborative Innovation Center of Atmospheric Environment and Equipment Technology, School of Environmental Science and Engineering, Nanjing University of Information Science & Technology, Nanjing, 210044, China
[c] University of Chinese Academy of Sciences, Beijing, 100049, China

ARTICLE INFO

Article history:
Received 15 September 2018
Received in revised form
22 December 2018
Accepted 30 January 2019
Available online 7 February 2019

Keywords:
Severe particulate pollution
T-PCA
Atmospheric circulation

ABSTRACT

This study examined the spatial and temporal variations of severe particulate pollution days (SPPDs) in China by using observed $PM_{2.5}$ concentrations during April 2013 to February 2018 from the Ministry of Environmental Protection of China. SPPDs were defined as those with observed daily mean $PM_{2.5}$ concentrations larger than 150 $\mu g\ m^{-3}$. Observations showed that northern China had the highest number of SPPDs during the studied period. Since 2015, the number of SPPDs in northwestern China is comparable to or even higher than that observed in Beijing-Tianjin-Hebei (BTH). The highest numbers of SPPDs observed within BTH and the Yangtze River Delta (YRD) were 122 (33), 95 (17), 57 (15), 78 (18), and 31 (25) days in 2013, 2014, 2015, 2016, and 2017, respectively, indicating a general decreasing trend as a result of emission reduction measures. SPPDs occurred mainly from November to February in BTH and in December and January in the YRD. The major circulation patterns associated with large-scale SPPDs were analyzed by using principal component analysis. Five typical synoptic weather patterns were identified for BTH. The most dominant weather type (a cold high centered over the Xinjiang and Mongolian regions) for BTH was also responsible for most of the SPPDs in the YRD. These results have important implications for emission control strategies during SPPDs. Emission control measures can be applied once the dominant circulation patterns have been predicted.

1. Introduction

Rapid economic growth and associated emissions have led to increases in aerosol concentrations in China in recent decades. Severe particulate pollution days (SPPDs) have been observed frequently in China with large anthropogenic emissions (Wang et al., 2014b) and unfavorable meteorological conditions (Wang et al., 2014a; Yang et al., 2016; Cai et al., 2017). Aerosol concentrations during SPPDs in January 2013 and December 2015 reached as high as 500 $\mu g\ m^{-3}$ (Wang et al., 2014a; Li et al., 2018). Such SPPDs caused substantial adverse effects on human health (Cohen et al., 2017; Zheng et al., 2017) and reduced atmospheric visibility (Sun et al., 2006; Cao et al., 2012). Understanding the spatial and temporal variations of severe particulate pollution events is essential for air quality planning in China.

Previous observational and modeling studies that examined severe particulate pollution in China were mostly focused on the physical and chemical mechanisms of a single episode. Ground-based observations reported peak $PM_{2.5}$ concentrations of 772 $\mu g\ m^{-3}$ in Beijing (Huang et al., 2014) and of 300 $\mu g\ m^{-3}$ in Shanghai (Andersson et al., 2015) in January 2013. Secondary aerosols, such as sulfate, nitrate, and secondary organic carbon, were found to contribute 30–77% to measured $PM_{2.5}$ concentrations during SPPDs (Huang et al., 2014). Recent studies suggested enhanced sulfate formation during SPPDs through heterogeneous reactions (Wang et al., 2014d) and the oxidation of SO_2 by NO_2 in

☆ This paper has been recommended for acceptance by Charles Wong.
* Corresponding author.
E-mail address: hongliao@nuist.edu.cn (H. Liao).

https://doi.org/10.1016/j.envpol.2019.01.124
0269-7491/

the aqueous phase (Cheng et al., 2016a; Wang et al., 2016). A number of studies also reported that stagnant weather conditions (characterized by reduced wind, a strong temperature inversion, and low boundary layer height) (Zhao et al., 2013), regional transport of pollutants (Zheng et al., 2015; Zheng et al., 2016), and aerosol-weather feedback (Wang et al., 2015; Qiu et al., 2017) were the major factors that caused the formation and maintains of SPPDs. However, to our knowledge, no previous studies have reported on the spatial and temporal variations of SPPDs in China.

There exist previous studies that examined temporal and spatial variations of air pollutants in recent years in China (Wang et al., 2014c;Zhang and Cao, 2015; Han et al., 2016; Cheng et al., 2016b; Song et al., 2017). Wang et al. (2014c) analyzed variations of six criteria pollutants (SO_2, NO_2, $PM_{2.5}$, PM_{10}, CO, and O_3) in 31 capital cities from March 2013 to February 2014 by using the hourly concentrations released by Ministry of Environmental Protection (MEP) of China. Zhang and Cao (2015), also by using the MEP data, investigated the spatiotemporal variations of $PM_{2.5}$ for 190 cities in 2014. Song et al. (2017) analyzed $PM_{2.5}$ concentrations in years of 2014–2016 from MEP, and reported that the annual mean $PM_{2.5}$ concentrations were decreasing nationwide but wintertime $PM_{2.5}$ levels were increasing in Northern China. These studies were focused on monthly, seasonal or annual mean concentrations and did not examine the frequency and intensity of severe particulate pollution in China.

Previous studies also attempted to identify the weather patterns that determined the high levels of air pollution. Zhang et al. (2012) used the T-mode principal component analysis (T-PCA) approach by using sea level pressure and obtained nine weather types in Beijing for years of 2000–2009. They discussed the characteristics of parameters such as atmospheric visibility, AOD, and PM_{10} under different weather patterns, and identified the weather conditions that were favorable to particulate pollution in Beijing. Zhang et al. (2016) classified 5 categories of weather conditions based on the Kirchhofer method by using geopotential height at 850 hPa altitude during 1980–2013 and found a stagnant weather condition that favored the accumulation of air pollutants in the North China Plain. Miao et al. (2017) carried out the T-PCA analysis by using geopotential height at 925 hPa and identified seven synoptic weather types over BTH during summertime from 2011 to 2014. They investigated the structure of planetary boundary layer and particulate matter pollution under different weather types. These studies, however, did not examine weather conditions conductive to SPPDs, which have important implications for controlling emissions during SPPDs.

The scientific goals of this study are as follows: 1) to examine the spatial distribution and temporal variation of SPPDs over China from April 2013 to February 2018 by using observed hourly $PM_{2.5}$ concentrations from MEP and 2) to identify the typical weather patterns that are responsible for SPPDs in BTH area and the YRD by using T-PCA approach. A severe particulate pollution day can be identified when the daily mean $PM_{2.5}$ concentration exceeds one concentration threshold. Following the study of Cai et al. (2017), the threshold of 150 $\mu g\,m^{-3}$ is used in this study, because the Chinese government issues a 'red alert' when the $PM_{2.5}$ concentration is forecast to exceed 150 $\mu g\,m^{-3}$ for 72 consecutive hours. Furthermore, according to the Air Quality Index (AQI, an integrated index calculated from daily concentrations of SO_2, NO_2, CO, O_3, PM_{10} and $PM_{2.5}$ measured at a monitoring station) of the Chinese MEP, air quality becomes heavily polluted when the AQI value is larger than 200, and the AQI of 200 corresponds to an observed $PM_{2.5}$ concentration of 150 $\mu g\,m^{-3}$ (http://kjs.mep.gov.cn/hjbhbz/bzwb/dqhjbh/dqhjzlbz/).

Section 2 presents the data and methods used in this study, including observed $PM_{2.5}$ concentrations in China, the T-PCA classification method to classify the synoptic weather patterns during SPPDs, and the backward trajectory analysis for identifying the origin of air masses in Beijing and Shanghai (two representative cities for BTH and the YRD, respectively). Section 3 presents the analysis of the spatial distribution and temporal variation of SPPDs over China. Section 4 examines the characteristics of SPPDs in BTH and YRD, and Section 5 shows the weather patterns that lead to SPPDs in BTH and YRD. The discussion and conclusions are presented in Section 6.

2. Data and methods

2.1. In situ measurements of $PM_{2.5}$

In January 2013, MEP started to release hourly concentrations of the six criteria pollutants (SO_2, NO_2, $PM_{2.5}$, PM_{10}, CO, and O_3), which have been widely used in previous studies (Wang et al., 2014c; Zhang and Cao, 2015; Song et al., 2017; Wang et al., 2017). Hourly $PM_{2.5}$ concentrations used in this study were downloaded from the MEP website http://106.37.208.233:20035/. $PM_{2.5}$ concentrations are measured by the micro-oscillating balance method and the β absorption method, following the China Environmental Protection Standard 'HJ 193–2013' and 'HJ 655–2013' (http://kjs.mep.gov.cn/hjbhbz/bzwb/jcffbz/201308/W020130802492823718666.pdf). Fig. S1 shows the spatial distribution of cities with hourly measured $PM_{2.5}$ concentrations in China. The observation network contained 74 cities in 2013, expanded to 190 cities in 2014, and has maintained 367 cities since 2015. Each city has several (a few to a dozen) monitoring sites with most of the sites located in urban areas. All downloaded concentrations for each site were selected based on the following steps: (1) data with negative or missing values are removed; (2) a site with less than 80% valid data since starting continuous observations is removed; and (3) the daily mean $PM_{2.5}$ concentration of the city is calculated only when there were more than 20 h of valid data during that day. Finally, 74 cities in 2013, 188 cities in 2014, and 362 cities from 2015 to 2017 are selected based on the >80% valid data criterion.

We examined the SPPDs in China by using hourly $PM_{2.5}$ concentrations from April 2013 to February 2018. We use the "season year", which includes four seasons starting from spring. Therefore, year 2013 covered April 2013 to February 2014, and each of the years 2014–2017 covered from March of that year to the February of the following year. Note that year 2013 had only 11 months because we collected the observational network data starting from April 2013.

2.2. HYSPLIT model

Backward trajectory analysis is carried out to investigate the potential source regions of air masses during SPPDs. The HYSPLIT model version 4.9, developed by the Air Resources Laboratory of the National Oceanic and Atmospheric Administration (NOAA ARL), is used to calculate backward trajectories for all the SPPDs that occurred from April 2013 to February 2018 in Beijing (116.4°E, 39.9°N) and Shanghai (121.3°E, 31.1°N). Four 72-h backward trajectories per day (00:00 06:00 12:00 18:00) at 500 m above ground level are computed for the two cities. Daily meteorological data are obtained from the global data assimilation system (GDAS) provided by the National Centers for Environmental Prediction (NCEP). The data contain 3-hourly meteorological fields on pressure levels with a spatial resolution of 1°. We use the MeteoInfo Software to conduct the Cluster analysis by examining the total spatial variance (TSV) (Wang, 2014).

2.3. Classification of circulation patterns for SPPDs

The obliquely rotated principal component analysis in the T-mode (T-PCA) is a commonly used tool for the classification of circulation patterns (Huth et al., 2008). The T-PCA calculates the eigenvectors of the input dataset by singular value decomposition and finds typical patterns by loadings that can be divided into classes (Miao et al., 2017). The application of the PCA in T-mode means that, in the input data matrix, daily patterns form the columns and grid-point values form its rows (Huth, 2000). This method has also been employed to investigate the circulation patterns that are conducive to particulate pollution in North China (Zhang et al., 2012; Miao et al., 2017) and the YRD (Xu et al., 2016). In this study, we use the cost733class software package (http://cost733.met.no) of T-PCA to identify the circulation patterns that caused SPPDs in BTH and YRD from April 2013 to February 2018. More details of T-PCA procedure in cost733class can be found in the Supplementary Material.

3. Spatiotemporal variations of SPPDs in China

3.1. Spatial distribution and trend in SPPDs

Fig. 1 shows the spatial distributions of annual SPPDs observed in China from 2013 to 2017. During all the years, SPPDs occurred more frequently in northern China than in southern China, which is consistent with the higher annual mean $PM_{2.5}$ concentrations in northern China than in southern China (Wang et al., 2017). The highest numbers of SPPDs observed within BTH (YRD) (see Fig. S1 for the domains) were 122 (33), 95 (17), 57 (15), 78 (18), and 31 (25) days in 2013, 2014, 2015, 2016, and 2017, respectively. Starting from 2015, cities in Xinjiang Autonomous Region in western China started to release $PM_{2.5}$ concentrations. SPPDs in northwestern China were comparable to or even higher than those observed in BTH. For example, at Kashi (76.0°E, 39.47°N) there were 108, 76, and 56 SPPDs in 2015, 2016, and 2017, respectively.

Fig. S2 presents the linear trends in annual SPPDs for 74 cities that had continuous measurements since 2013. All cities, except for Xi'an (108.94°E, 34.28°N), Taiyuan (112.55°E, 37.87°N), and Urumchi (87.62°E, 43.83°N), exhibited decreasing trends of SPPDs during 2013–2017, which demonstrates that the Air Pollution Prevention and Control Action Plan released by the Chinese government in 2012 has improved air quality over the past several years. The trends exceeding -10 days yr^{-1} are found in approximately half of the cities in BTH, with a maximum value of -22.2 days yr^{-1} in Xingtai City (114.50°E, 37.07°N). There was only a small decreasing trend in the number of SPPDs for Beijing. SPPDs in Beijing were 32, 39, 36, 46, and 8 days in 2013, 2014, 2015, 2016, and 2017, respectively, producing a linear trend of -4.1 days yr^{-1}. In the YRD, the trends in the number of SPPDs were in the range of $-2 \sim -6$ days yr^{-1}.

3.2. Seasonal variations in SPPDs

Fig. S3 shows the seasonal distributions of observed SPPDs in China from 2013 to 2017. For cities in central China (Hebei, Henan, and Shandong provinces), the frequency of SPPDs was the highest

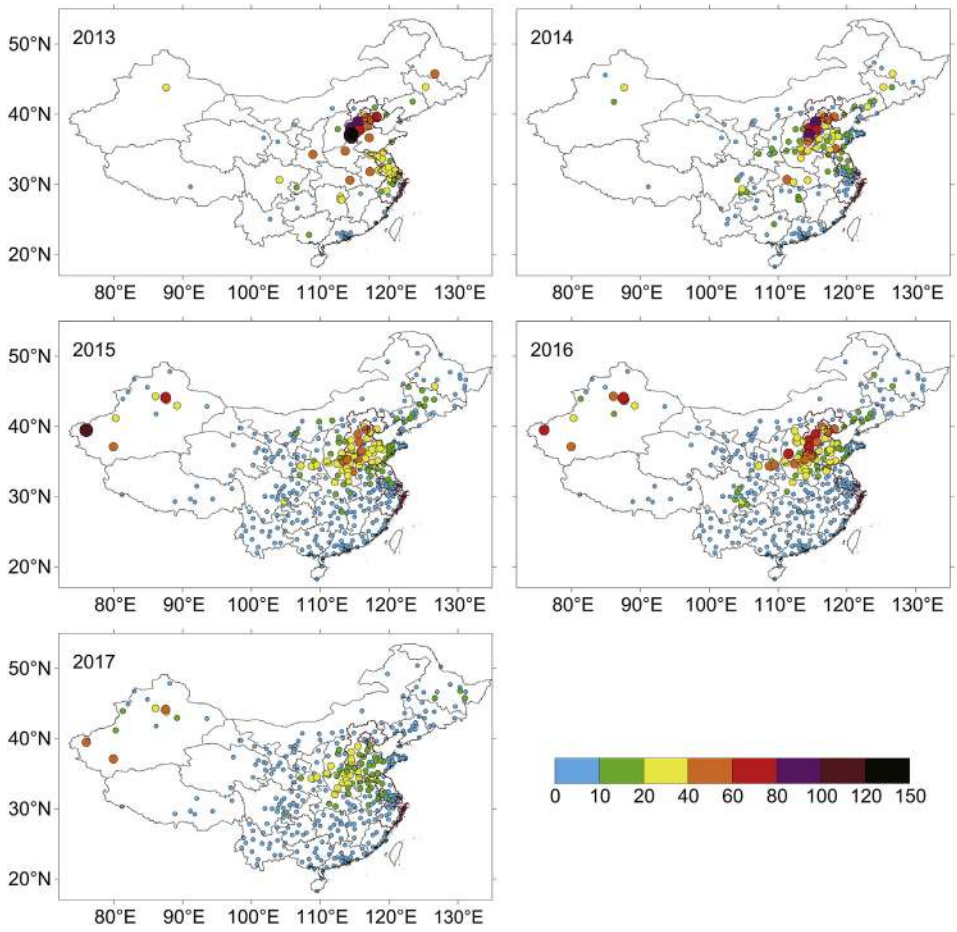

Fig. 1. Spatial distributions of observed SPPDs (unit: days yr^{-1}) in China from 2013 to 2017.

in December-January-February (DJF), followed by September-October-November (SON) and March-April-May (MAM). Cities in northeastern China (Liaoning, Jining, and Heilongjiang provinces) experienced more SPPDs in SON than in DJF in 2014, 2015 and 2017 because of more stagnant days in SON than in DJF (Huang et al., 2017) and intensive coal combustion (northeastern cities begin to use heating in early SON due to the high latitudes). For cities in northwestern China, SPPDs occurred mostly in DJF and MAM, which can be explained by the large anthropogenic emissions in DJF (Mamtimin and Meixner, 2011) and dust events in MAM (Zhang and Cao, 2015). Among all the seasons, June-July-August (JJA) had the lowest number of SPPDs over the past five years.

3.3. Intensity of pollution on SPPDs

Fig. 2 shows the spatial distribution of the intensity of pollution on SPPDs. For each city, the intensity is calculated as the average of the peak-hour $PM_{2.5}$ concentration on all SPPDs identified from the measurements available during 2013–2017. During MAM, cities in western China were influenced by dust events, leading to the highest $PM_{2.5}$ concentrations of 500–600 $\mu g\,m^{-3}$. In JJA, the averaged peak $PM_{2.5}$ concentrations in BTH were in the range of 250–300 $\mu g\,m^{-3}$. For SON, the maximum concentrations of $PM_{2.5}$ of 500–600 $\mu g\,m^{-3}$ were found in northeastern China. During DJF, peak $PM_{2.5}$ concentrations were approximately 300–400 $\mu g\,m^{-3}$ in the cities north of 34°N. Peak $PM_{2.5}$ concentrations in most cities in southern China (south of 34°N) were lower than those in northern China (approximately 200–300 $\mu g\,m^{-3}$ for most cities). The abnormally high values in several cities over Fujian, Guangdong, and Guangxi during DJF were caused by fireworks during Chinese Spring Festival.

4. SPPDs in BTH and the YRD

4.1. Annual cycle and interannual variation

Fig. S4 shows the annual cycles of SPPDs in BTH and the YRD. SPPDs in BTH (YRD) are averaged over the 10 cities (26 cities) shown in Fig. S1. When averaged over BTH (YRD), there were 72 (20), 60 (7), 36 (6), 51 (3), and 17 (5) SPPDs in 2013, 2014, 2015, 2016, and 2017, respectively. In BTH, SPPDs occurred mainly from November to February, which is consistent with the heating period in North China. In this region, SPPDs occurred on approximately half of the days in December during 2013, 2015 and 2016. In 2014, the number of SPPDs in BTH was the highest in October, which might have been caused by open biomass burning (Long et al., 2016). The number of SPPDs in October in BTH has decreased since 2015 as a result of the restriction of open biomass burning in recent years. SPPDs in the YRD occurred mainly in December and January. The SPPDs during these two months accounted for approximately 90% of the annual SPPDs.

Fig. 3 displays the yearly variations in seasonal SPPDs in BTH and the YRD. Over BTH, the number of SPPDs in MAM, JJA, and SON had a decreasing trend, and those in DJF showed a 'U' shape (with no significant improvement) from 2013 to 2016 and a large decrease in 2017. Over the YRD, the SPPDs in MAM and SON lasted for approximately

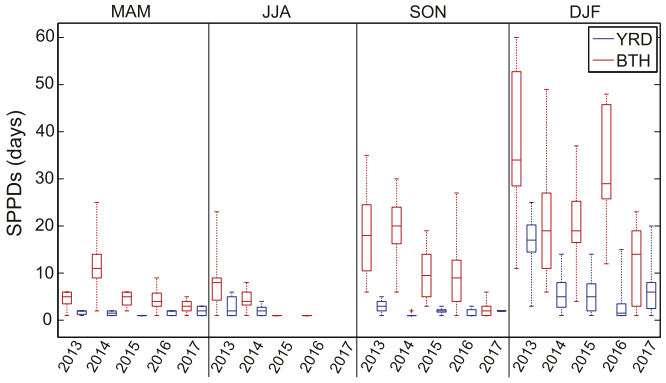

Fig. 3. Interannual variation of SPPDs in BTH (10 cities) and the YRD (26 cities) from April 2013 to February 2018. The whisker and box show the minimum (maximum) value and 25% (75%) percentiles, respectively.

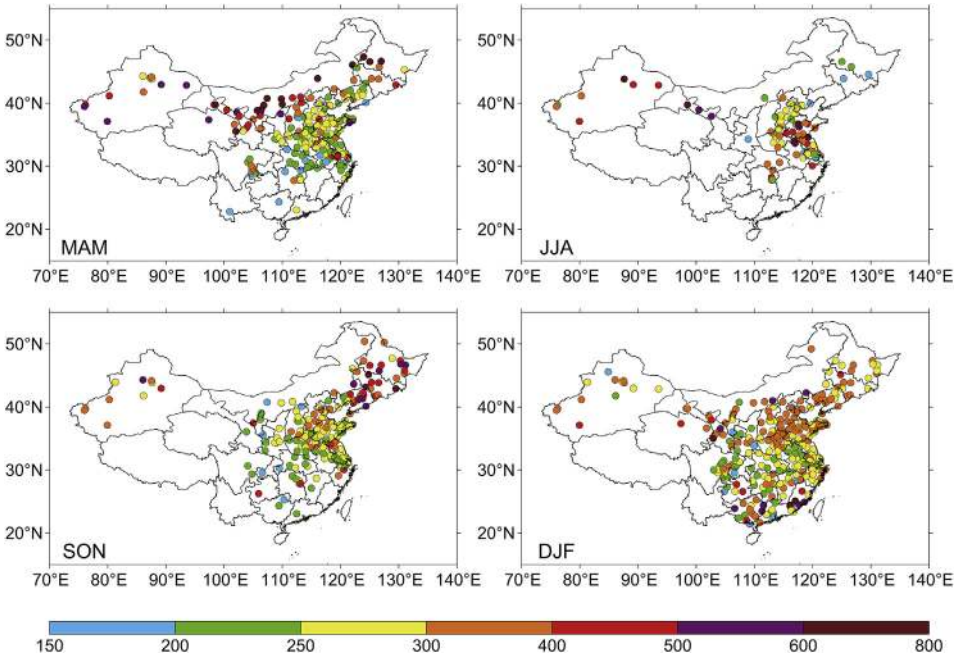

Fig. 2. Spatial distributions of the averaged intensity of pollution on SPPDs. For each city, the intensity is calculated as the average of the peak-hour $PM_{2.5}$ concentration (unit: $\mu g\,m^{-3}$) on all SPPDs identified from the measurements available from April 2013 to February 2018.

1–2 days from 2013 to 2017. SPPDs have not been observed during JJA since 2015. During DJF, the number of SPPDs in the YRD showed large decreases from 16 days in 2013 to 3–6 days in 2014–2017. The anthropogenic emissions of major air pollutants in China decreased from 2013 to 2017 (Zheng et al., 2018), therefore the increase in SPPDs during DJF in BTH from 2014 to 2015 and 2016, as well as the relatively high frequency of SPPDs during DJF in YRD in 2015 and 2017, indicate the role of climate in the formation of SPPDs. Based on ground observations, Chang et al. (2016) suggested that the El Nino event in 2015 led to a large increase of 80–100 $\mu g\ m^{-3}$ in $PM_{2.5}$ concentrations in the North China Plain (NCP) in December 2015, which contributed to the high number of SPPDs in BTH in December 2015 (Fig. S4). Zhao et al. (2018) reported that $PM_{2.5}$ concentrations in NCP reduced by 100–200 $\mu g\ m^{-3}$ under strong Siberian High conditions (for example, in January 2016) on the basis of WRF-Chem simulations. Yin and Wang (2017) reported that the positive phase of the East Atlantic-West Russia pattern in the middle troposphere in December 2016 led to unfavorable meteorological conditions and a high number of SPPDs in North China. Therefore, variability in meteorology can influence SPPDs on subseasonal and interannual timescales.

4.2. Persistence of severe particulate pollution episodes (SPPEs)

SPPDs are classified as SPPEs based on their duration with daily averaged $PM_{2.5}$ concentration larger than 150 $\mu g\ m^{-3}$. Over BTH and the YRD, SPPEs usually lasted 1–7 days. From April 2013 to February 2018, the frequency of episodes with a persistence of 1–7 days for BTH or YRD can be calculated as follows:

$$F_{i,j} = \frac{\sum_{k=1}^{n} D_{i,j,k}}{\sum_{i=1}^{4}\sum_{j=1}^{7}\sum_{k=1}^{n} D_{i,j,k}} * 100\%, \quad (1)$$

where $F_{i,j}$ is the frequency of episodes that last for j day (or days) in season i in BTH (or YRD). $D_{i,j,k}$ is the number of episodes that last for j day (or days) in season i in city k of BTH (or YRD) from April 2013 to February 2018. The denominator is the total number of episodes in the region. From April 2013 to February 2018, there were 1063 SPPEs in 10 cities in BTH (Fig. 4), in which 72.0% and 28.0% of episodes lasted for 1–2 days and ≥3 days, respectively. SPPEs with a persistence of 4 days or longer occurred mainly during DJF. Over the same time period, there were 612 SPPEs in 26 cities on the YRD (Fig. 4), in which 85.2% and 14.8% of episodes lasted for 1–2 days and ≥3 days, respectively.

5. Circulation patterns conducive to SPPDs in BTH and the YRD

To identify the typical circulation patterns that were conducive to SPPDs in BTH and the YRD, sea level pressure (SLP), geopotential height (HGT), winds at 10 m, 850 hPa, and 500 hPa altitudes, temperature and relative humidity at 27 pressure levels from the surface to 100 hPa altitude were obtained from ERA-Interim datasets for the period of 2013–2018 to constitute daily series used by the obliquely rotated T-mode PCA method and composite analysis. We examined the typical circulation pattern for large-scale SPPDs (for each large-scale SPPD, more than half of the cities in BTH or the YRD experienced severe particulate pollution) for the months with the highest number of SPPDs (October to February in BTH, and December to February in the YRD, as shown in Fig. S4).

5.1. Dominant synoptic weather patterns for SPPDs in BTH

From April 2013 to February 2018, 237 large-scale SPPDs occurred in BTH, of which 199 occurred from October to February. Using the T-PCA classification approach, 5 dominant types of synoptic weather patterns are identified for BTH in these months. Table S1 summarizes the frequency and average values of the observed meteorological parameters of the five dominant synoptic weather patterns identified for BTH. The order of type 1 to type 5 listed in Table S1 was determined by the amount of explained variances (Miao et al., 2017). Types 2 and 3 are the dominant weather patterns in BTH, and were responsible for 35.7% and 31.2%, respectively, of the 199 large-scale SPPDs in BTH. Types 1, 4 and 5 have small percentages of 12.1%, 16.6% and 4.4%, respectively. Fig. 5 presents the composite figures of SLP and 10-m winds, geopotential height at 850 hPa and 500 hPa with corresponding winds, as well as the pressure-longitude cross sections of temperature and relative humidity averaged over the latitudes of 37–41°N for the five typical circulation patterns.

Fig. 5a shows the locations of high and low pressure at sea level for the five typical circulation patterns. In type 1, the Siberian Cold High is anomalously weak and a weak high is centered over the Sea of Japan. For type 2, a strong cold high with a central pressure of 1038 hPa is located over Mongolia and moves eastward and passes through Northern China. BTH is located within the southern part of this high. In type 3, the cold high is weak and extends from Xinjiang autonomous region to the entire middle section of China. The whole of eastern China has uniform pressure and therefore a small pressure gradient, leading to weak winds that are favorable for the formation of SPPDs. In type 4, the Siberian High with a central pressure of 1040 hPa extends to northeastern China, and its southeast edge influences BTH with relatively weak northwesterlies. In type 5, the Siberian High is weaker than in type 4, with few impacts on eastern China. Under the type 5 circulation pattern, BTH is influenced by a weak high pressure centered over the Korean Peninsula, which leads to southerlies and southeasterlies in BTH.

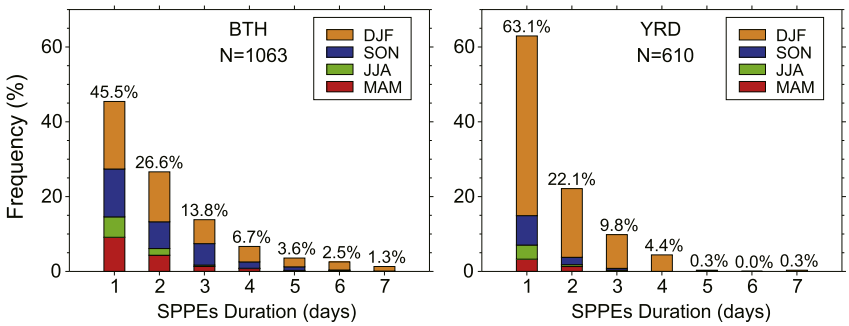

Fig. 4. Frequency of SPPEs with a persistence of 1–7 days for BTH and the YRD from April 2013 to February 2018. There were 1063 SPPEs in 10 cities in BTH and 610 SPPEs in 26 cities in the YRD.

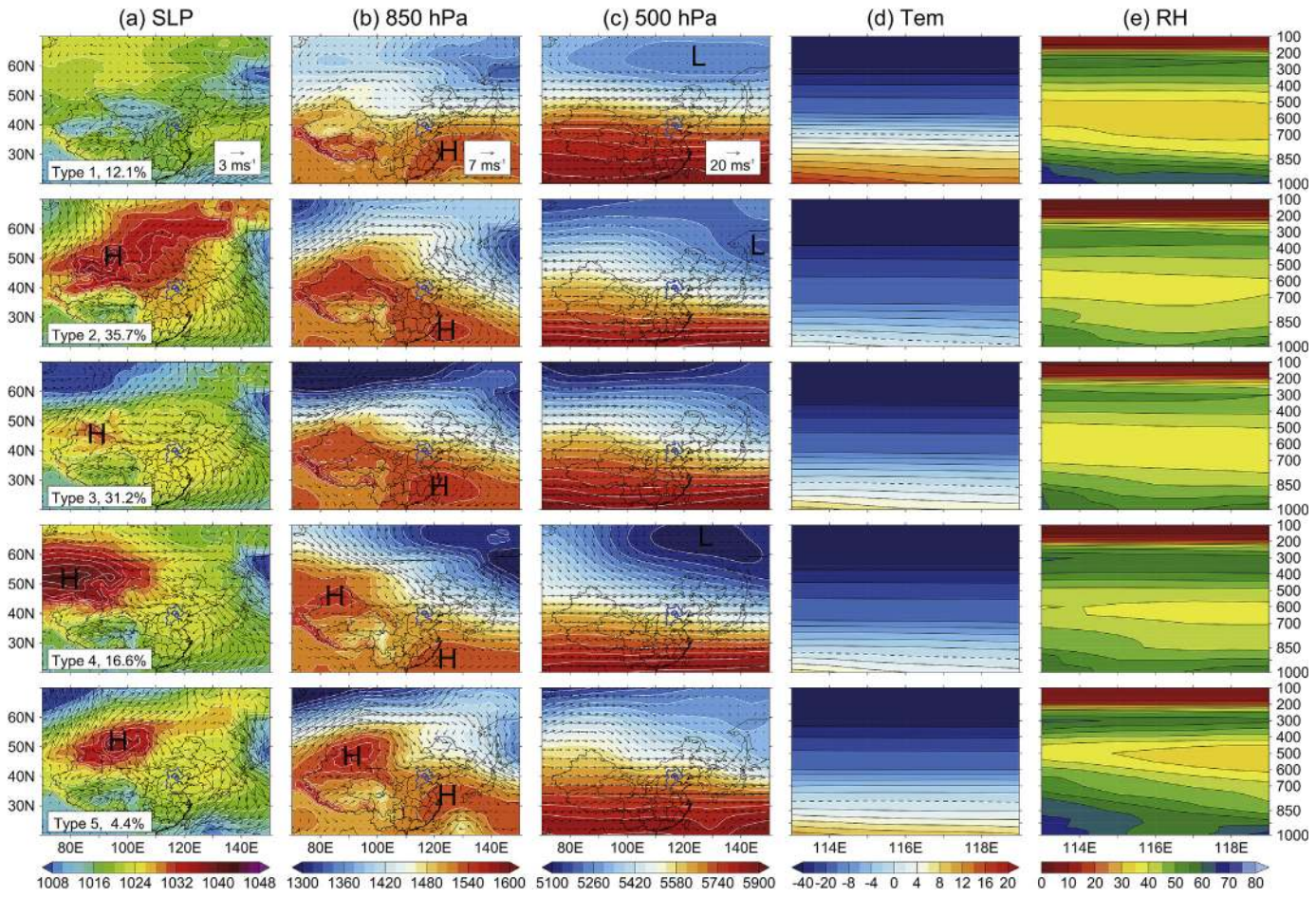

Fig. 5. Weather patterns for BTH. (a) sea level pressure and wind field at 10 m, (b) geopotential height and wind field at 850 hPa, (c) geopotential height and wind field at 500 hPa, (d) pressure-longitude cross section of temperature (unit: °C), and (e) pressure-longitude cross section of relative humidity (unit: %). The cross sections are averaged over 37–41°N. The bold blue line indicates the boundary of BTH. (For interpretation of the references to colour in this figure legend, the reader is referred to the Web version of this article.)

An anticyclone is located over the East China Sea at 850 hPa in all of the circulation types (Fig. 5b). The accompanied southerlies in eastern China weaken the East Asian Winter Monsoon (EAWM) and enhance the transport of moist air from southern China, which favors the formation of secondary aerosols. At 500 hPa (Fig. 5c), a weak East Asia trough is identified in all five patterns. The meridional winds are relatively weak and westerlies prevail in northern China. As a result, the cold and dry northwesterlies have difficulty reaching BTH, which favors the maintenance of SPPDs.

Fig. S5 shows the same meteorological fields as in Fig. 5 but for anomalies of these fields with respect to the means over 1988–2017. Anomalous southerlies are identified over BTH at 850 hPa and SLP. The anomalous southerlies reduce the prevailing northwesterlies in the lower troposphere (850 hPa), leading to weak winds (approximately 1.5 m s^{-1} for all types in Table S1) at the surface during SPPDs. Anomalous southerlies over BTH at 850 bring warm and moist air that favors chemical formation of secondary aerosols. The temperature anomaly around 850 hPa is higher than at the surface (Fig. S5d), which is a stable condition that leads to the accumulation of $PM_{2.5}$. We also examined the weather patterns for none-SPPDs and found that the weather types mentioned above were sufficient and necessary conditions for SPPDs (see supplementary).

Transport trajectories of air pollutants are influenced by synoptic systems (Shu et al., 2017). Fig. S10 shows the calculated clusters of backward trajectories of the five circulation patterns for SPPDs in Beijing from April 2013 to February 2018. In winter, the Siberian High appears over the Asian Continent with a strong Aleutian Low to its east, which is the most prominent feature of the EAWM. Therefore, strong northwesterlies prevail along the eastern flank of the Siberian High and the East Asian Coast (Gong et al., 2001; Hao et al., 2016). However, air masses above 1500 m were mainly from the northwest and west of BTH for all five circulation types (Fig. S10). This indicates fewer cold and dry northwesterly intrusions occurring in BTH, which is consistent with the westerlies at 500 hPa presented in Fig. 5c. In addition, there was a cluster of southerlies (accounting for 62.5%, 51.0%, 10.8%, 34.1%, and 59.4% for types 1, 2, 3, 4, and 5, respectively) within the PBL (under 1000 m) with low wind speeds in all patterns. This suggests that the transport of air pollutant from nearby areas south of Beijing is important when the city experiences SPPDs.

5.2. Predominant synoptic weather patterns for SPPDs in the YRD

From April 2013 to February 2018, 21 large-scale SPPDs occurred in the YRD and all occurred in the selected most polluted months from December to February. Because there are not enough samples to analyze the circulation patterns, we conduct a composite analysis for the YRD. Fig. S11 presents composite figures of SLP, GHT, and winds at 850 and 500 hPa for the 21 large-scale SPPDs that occurred

in the YRD. During SPPDs, the Siberian High is centered over the Xinjiang and Mongolian regions with a central pressure of 1038 hPa at the sea level. The weak pressure gradient in eastern China leads to relatively low wind speed. At 850 hPa, the northwesterlies prevail over the YRD. As a result, air masses were mainly from northern China, which transported pollutants to the YRD as they passed through polluted regions, such as BTH and Shandong Province. At 500 hPa, the YRD was under the influence of westerlies, indicating a stable circulation pattern with weak cold air intrusion. Hence, the warm (Fig. S12d) conditions within PBL is beneficial for local pollutions.

Fig. S13 presents the clusters of 72-h backward trajectories during large-scale SPPDs in Shanghai. Up to 51.9% of the air masses were from northern China with a height below 1500 m. These airflows were related to long-range transport within the PBL from the polluted areas (BTH and Shandong Province) to the YRD. Furthermore, a cluster (accounting for 30.8%) between 500 and 1000 m with low wind speed indicated local transport of air pollutants during SPPDs. The circulation pattern for SPPDs in the YRD is similar to type 2 for BTH.

6. Discussion and conclusions

The spatial distribution, temporal variation, and intensity of SPPDs (days with observed $PM_{2.5}$ concentrations larger than 150 $\mu g\,m^{-3}$) over China were investigated using observed $PM_{2.5}$ concentrations from April 2013 to February 2018. Results show that northern China had the highest number of SPPDs over the past five years. Attention should also be paid to northwestern China where the number of SPPDs was comparable to or even higher than that observed in BTH. As a result of emission control strategies, most sites in China exhibited decreasing linear trends in annual SPPDs during 2013–2017.

The highest number of SPPDs observed within BTH (YRD) was 122 (33), 95 (17), 57 (15), 78 (18), and 31 (25) days in 2013, 2014, 2015, 2016, and 2017, respectively. SPPDs occurred mainly from November to February in BTH and during December and January in the YRD. SPPDs had large interannual variation during winter, especially in BTH, which was influenced by variability in meteorology. During the studied period, 72.0% and 28.0% of SPPEs in the BTH lasted for 1–2 days and ≥3 days, respectively, while 85.2% and 14.8% of SPPEs in the YRD lasted for 1–2 days and ≥3 days, respectively.

The major circulation types associated with large-scale SPPDs were analyzed using the T-PCA classification method. From October to February, five typical synoptic weather patterns were classified for BTH. The most dominant pattern (type 2) is characterized by a strong cold high with a central sea level pressure of 1038 hPa located over Mongolia, which moves eastward passing through Northern China. The second dominant pattern (type 3) is characterized by a weak cold high that extends from Xinjiang to the entire middle part of China, leading to a small pressure gradient in eastern China. These two types were responsible for 35.7% and 31.2%, respectively, of the 199 large-scale SPPDs in BTH. The most dominant weather type (type 2) for BTH was also responsible for most of the 21 large-scale SPPDs in the YRD. Back trajectory analysis was also carried out to understand the transport pathways of pollutants during SPPDs. The transport of air pollutants from nearby areas south of Beijing contributed to the SPPDs in Beijing, and those in Shanghai were influenced by air masses that passed via the heavily polluted BTH and Shandong Province. These results have important implications for emission control strategies during SPPDs. Emission control measures can be applied along the air mass pathways when the dominant circulation patterns have been predicted.

Acknowledgments

This work was supported by the National Natural Science Foundation of China under grants 41475137, 91544219, and 91744311.

Appendix A. Supplementary data

Supplementary data to this article can be found online at https://doi.org/10.1016/j.envpol.2019.01.124.

References

Andersson, A., Deng, J.J., Du, K., Zheng, M., Yan, C.Q., Skold, M., Gustafsson, O., 2015. Regionally-varying combustion sources of the January 2013 severe haze events over eastern China. Environ. Sci. Technol. 49, 2038–2043.
Cai, W.J., Li, K., Liao, H., Wang, H.J., Wu, L.X., 2017. Weather conditions conducive to Beijing severe haze more frequent under climate change. Nat. Clim. Change 7, 257–262.
Cao, J.J., Wang, Q.Y., Chow, J.C., Watson, J.G., Tie, X.X., Shen, Z.X., Wang, P., An, Z.S., 2012. Impacts of aerosol compositions on visibility impairment in Xi'an, China. Atmos. Environ. 59, 559–566.
Chang, L.Y., Xu, J.M., Tie, X.X., Wu, J.B., 2016. Impact of the 2015 El Nino event on winter air quality in China. Sci. Rep. 6, 34275.
Cheng, Y.F., Zheng, G.J., Wei, C., Mu, Q., Zheng, B., Wang, Z.B., Gao, M., Zhang, Q., He, K.B., Carmichael, G., Pöschl, U., Su, H., 2016a. Reactive nitrogen chemistry in aerosol water as a source of sulfate during haze events in China. Sci. Adv. 2 (12).
Cheng, Z., Luo, L., Wang, S., Wang, Y., Sharma, S., Shimadera, H., Wang, X., Bressi, M., de Miranda, R.M., Jiang, J., Zhou, W., Fajardo, O., Yan, N., Hao, J., 2016b. Status and characteristics of ambient $PM_{2.5}$ pollution in global megacities. Environ. Int. 89–90, 212–221.
Cohen, A.J., Brauer, M., Burnett, R., Anderson, H.R., Frostad, J., Estep, K., Balakrishnan, K., Brunekreef, B., Dandona, L., Dandona, R., Feigin, V., Freedman, G., Hubbell, B., Jobling, A., Kan, H., Knibbs, L., Liu, Y., Martin, R., Morawska, L., Pope, C.A., Shin, H., Straif, K., Shaddick, G., Thomas, M., van Dingenen, R., van Donkelaar, A., Vos, T., Murray, C.J.L., Forouzanfar, M.H., 2017. Estimates and 25-year trends of the global burden of disease attributable to ambient air pollution: an analysis of data from the Global Burden of Diseases Study 2015. Lancet 389, 1907–1918.
Gong, D.Y., Wang, S.W., Zhu, J.H., 2001. East Asian winter monsoon and Arctic oscillation. Geophys. Res. Lett. 28 (10), 2073–2076.
Han, R., Wang, S., Shen, W., Wang, J., Wu, K., Ren, Z., Feng, M., 2016. Spatial and temporal variation of haze in China from 1961 to 2012. J. Environ. Sci. 46, 134–146.
Hao, X., Li, F., Sun, J.Q., Wang, H.J., He, S.P., 2016. Assessment of the response of the East Asian winter monsoon to ENSO-like SSTAs in three U.S. CLIVAR Project models. 2016. Int. J. Climatol. 36, 847–866.
Huang, Q.Q., Cai, X.H., Song, Y., Zhu, T., 2017. Air stagnation in China (1985–2014): climatological mean features and trends. Atmos. Chem. Phys. 17, 7793–7805.
Huang, R.J., Zhang, Y., Bozzetti, C., Ho, K.F., Cao, J.J., Han, Y., Daellenbach, K.R., Slowik, J.G., Platt, S.M., Canonaco, F., Zotter, P., Wolf, R., Pieber, S.M., Bruns, E.A., Crippa, M., Ciarelli, G., Piazzalunga, A., Schwikowski, M., Abbaszade, G., Schnelle-Kreis, J., Zimmermann, R., An, Z., Szidat, S., Baltensperger, U., El Haddad, I., Prevot, A.S., 2014. High secondary aerosol contribution to particulate pollution during haze events in China. Nature 514, 218–222.
Huth, R., 2000. A circulation classification scheme applicable in GCM studies. Theor. Appl. Climatol. 67 (1–2), 1–18.
Huth, R., Beck, C., Philipp, A., Demuzere, M., Ustrnul, Z., Cahynova, M., Kysely, J., Tveito, O.E., 2008. Classifications of atmospheric circulation patterns: recent advances and applications. Ann. N. Y. Acad. Sci. 1146, 105–152.
Li, K., Liao, H., Cai, W.J., Yang, Y., 2018. Attribution of anthropogenic influence on atmospheric patterns conducive to recent most severe haze over eastern China. Geophys. Res. Lett. 45 (4), 2072–2081.
Long, X., Tie, X.X., Cao, J.J., Huang, R.J., Feng, T., Li, N., Zhao, S.Y., Tian, J., Li, G.H., Zhang, Q., 2016. Impact of crop field burning and mountains on heavy haze in the North China Plain: a case study. Atmos. Chem. Phys. 16, 9675–9691.
Mamtimin, B., Meixner, F.X., 2011. Air pollution and meteorological processes in the growing dryland city of Urumqi (Xinjiang, China). Sci. Total Environ. 409, 1277–1290.
Miao, Y.C., Guo, J.P., Liu, S.H., Liu, H., Li, Z.Q., Zhang, W.C., Zhai, P.M., 2017. Classification of summertime synoptic patterns in Beijing and their associations with boundary layer structure affecting aerosol pollution. Atmos. Chem. Phys. 17, 3097–3110.
Qiu, Y.L., Liao, H., Zhang, R.J., Hu, J.L., 2017. Simulated impacts of direct radiative effects of scattering and absorbing aerosols on surface layer aerosol concentrations in China during a heavily polluted event in February 2014. J. Geophys. Res. Atmos. 122, 5955–5975.
Shu, L., Xie, M., Gao, D., Wang, T.J., Fang, D.X., Liu, Q., Huang, A.N., Peng, L.W., 2017. Regional severe particle pollution and its association with synoptic weather patterns in the Yangtze River Delta region, China. Atmos. Chem. Phys. 12871–12891.

Song, C.B., Wu, L., Xie, Y.C., He, J.J., Chen, X., Wang, T., Lin, Y.C., Jin, T.S., Wang, A.X., Liu, Y., Dai, Q.L., Liu, B.S., Wang, Y.N., Mao, H.J., 2017. Air pollution in China: status and spatiotemporal variations. Environ. Pollut. 227, 334–347.

Sun, Y.L., Zhuang, G.S., Tang, A.H., Wang, Y., An, Z.S., 2006. Chemical characteristics of $PM_{2.5}$ and PM_{10} in haze-fog episodes in Beijing. Environ. Sci. Technol. 40, 3148–3155.

Wang, G.H., Zhang, R.Y., Gomez, M.E., Yang, L.X., Levy Zamora, M., Hu, M., Lin, Y., Peng, J.F., Guo, S., Meng, J.J., Li, J.J., Cheng, C.L., Hu, T.F., Ren, Y.Q., Wang, Y.S., Gao, J., Cao, J.J., An, Z.S., Zhou, W.J., Li, G.H., Wang, J.Y., Tian, P.F., Marrero-Ortiz, W., Secrest, J., Du, Z.F., Zheng, J., Shang, D.J., Zeng, L.M., Shao, M., Wang, W.G., Huang, Y., Wang, Y., Zhu, Y.J., Li, Y.X., Hu, J.X., Pan, B.W., Cai, L., Cheng, Y.T., Ji, Y.M., Zhang, F., Rosenfeld, D., Liss, P.S., Duce, R.A., Kolb, C.E., Molina, M.J., 2016. Persistent sulfate formation from London Fog to Chinese haze. Proc. Natl. Acad. Sci. U.S.A. 113, 13630–13635.

Wang, H., Xu, J.Y., Zhang, M., Yang, Y.Q., Shen, X.J., Wang, Y.Q., Chen, D., Guo, J.P., 2014a. A study of the meteorological causes of a prolonged and severe haze episode in January 2013 over central-eastern China. Atmos. Environ. 98, 146–157.

Wang, H., Shi, G.Y., Zhang, X.Y., Gong, S.L., Tan, S.C., Chen, B., Che, H.Z., Li, T., 2015. Mesoscale modelling study of the interactions between aerosols and PBL meteorology during a haze episode in China Jing–Jin–Ji and its near surrounding region – Part 2: aerosols' radiative feedback effects. Atmos. Chem. Phys. 15, 3277–3287.

Wang, J.D., Zhao, B., Wang, S.X., Yang, F.M., Xing, J., Morawska, L., Ding, A.J., Kulmala, M., Kerminen, V.M., Kujansuu, J., Wang, Z.F., Ding, D., Zhang, X.Y., Wang, H.B., Tian, M., Petaja, T., Jiang, J.K., Hao, J.M., 2017. Particulate matter pollution over China and the effects of control policies. Sci. Total Environ. 584–585, 426–447.

Wang, S.X., Zhao, B., Cai, S.Y., Klimont, Z., Nielsen, C.P., Morikawa, T., Woo, J.H., Kim, Y., Fu, X., Xu, J.Y., Hao, J.M., He, K.B., 2014b. Emission trends and mitigation options for air pollutants in East Asia. Atmos. Chem. Phys. 14, 6571–6603.

Wang, Y.G., Ying, Q., Hu, J.L., Zhang, H.L., 2014c. Spatial and temporal variations of six criteria air pollutants in 31 provincial capital cities in China during 2013-2014. Environ. Int. 73, 413–422.

Wang, Y.X., Zhang, Q.Q., Jiang, J.K., Zhou, W., Wang, B.Y., He, K.B., Duan, F.K., Zhang, Q., Philip, S., Xie, Y.Y., 2014d. Enhanced sulfate formation during China's severe winter haze episode in January 2013 missing from current models. J. Geophys. Res. Atmos. 119, 10,425-410,440.

Wang, Y.Q., 2014. MeteoInfo: GIS software for meteorological data visualization and analysis. Meteorol. Appl. 21 (2), 360–368.

Xu, J.M., Chang, L.Y., Qu, Y.H., Yan, F.X., Wang, F.Y., Fu, Q.Y., 2016. The meteorological modulation on $PM_{2.5}$ interannual oscillation during 2013 to 2015 in Shanghai, China. Sci. Total Environ. 572, 1138–1149.

Yang, Y., Liao, H., Lou, S.J., 2016. Increase in winter haze over eastern China in recent decades: roles of variations in meteorological parameters and anthropogenic emissions. J. Geophys. Res. Atmos. 121, 13,050–013,065.

Yin, Z.C., Wang, H.J., 2017. Role of atmospheric circulations in haze pollution in December 2016. Atmos. Chem. Phys. 11673–11681.

Zhang, J.P., Zhu, T., Zhang, Q.H., Li, C.C., Shu, H.L., Ying, Y., Dai, Z.P., Wang, X., Liu, X.Y., Liang, A.M., Shen, H.X., Yi, B.Q., 2012. The impact of circulation patterns on regional transport pathways and air quality over Beijing and its surroundings. Atmos. Chem. Phys. 12, 5031–5053.

Zhang, Y., Ding, A., Mao, H., Nie, W., Zhou, D., Liu, L., Huang, X., Fu, C., 2016. Impact of synoptic weather patterns and inter-decadal climate variability on air quality in the North China Plain during 1980–2013. Atmos. Environ. 124, 119–128.

Zhang, Y.L., Cao, F., 2015. Fine particulate matter ($PM_{2.5}$) in China at a city level. Sci. Rep. 5, 14884.

Zhao, S.Y., Feng, T., Tie, X.X., Long, X., Li, G.H., Cao, J.J., Zhou, W.J., An, Z.S., 2018. Impact of climate change on Siberian High and wintertime air pollution in China in past two decades. Earth's Future 6, 118–133.

Zhao, X.J., Zhao, P.S., Xu, J., Meng, W., Pu, W.W., Dong, F., He, D., Shi, Q.F., 2013. Analysis of a winter regional haze event and its formation mechanism in the North China Plain. Atmos. Chem. Phys. 13, 5685–5696.

Zheng, B., Tong, D., Li, M., Liu, F., Hong, C., Geng, G., Li, H., Li, X., Peng, L., Qi, J., Yan, L., Zhang, Y., Zhao, H., Zheng, Y., He, K., Zhang, Q., 2018. Trends in China's anthropogenic emissions since 2010 as the consequence of clean air actions. Atmos. Chem. Phys. 18, 14095–14111.

Zheng, G.J., Duan, F.K., Su, H., Ma, Y.L., Cheng, Y., Zheng, B., Zhang, Q., Huang, T., Kimoto, T., Chang, D., Pöschl, U., Cheng, Y.F., He, K.B., 2015. Exploring the severe winter haze in Beijing: the impact of synoptic weather, regional transport and heterogeneous reactions. Atmos. Chem. Phys. 15, 2969–2983.

Zheng, G.J., Duan, F.K., Ma, Y.L., Zhang, Q., Huang, T., Kimoto, T., Cheng, Y.F., Su, H., He, K.B., 2016. Episode-based evolution pattern analysis of haze pollution: method development and results from Beijing, China. Environ. Sci. Technol. 50, 4632–4641.

Zheng, Y., Xue, T., Zhang, Q., Geng, G.N., Tong, D., Li, X., He, K.B., 2017. Air quality improvements and health benefits from China's clean air action since 2013. Environ. Res. Lett. 12, 114020.